Supplementary information for

Structure distortion induced monoclinic sodium iron hexacyanoferrate as high-performance electrode for rocking-chair desalination battery

Yuliang Wu [a], Junkun Huang [a], Chaolin Li [a, b], Wenhui Wang [a, b*]

a School of Civil and Environmental Engineering, Harbin Institute of Technology, Shenzhen, Shenzhen 518055, China

b State Key Laboratory of Urban Water Resource and Environment, Harbin Institute of Technology, Harbin, 150090, China

* Corresponding author. E-mail: wangwenhui@hit.edu.cn.

Material preparation

Sodium iron hexacyanoferrate (NaFeHCF) powders were produced by a controlled coprecipitation method. Typically, 0.2 mol of sodium ferricyanide decahydrate and 10 mg of ascorbic acid, and 0.2 mol of ferrous chloride and 10 mg of ascorbic acid were dissolved in 100 mL deionized water to form solution A and B, respectively. 0.1 mol/L of sodium citrate and 1.0 mol/L of sodium chloride were dissolved in 100 mL deionized water to form solution C under stirring at 500 rpm, which was then kept the temperature at 60˚C. Subsequently, solutions A and B were added to solution C at the rate of 100 mL/h to obtain a mixed solution and kept stirring for 24 h. The precipitated product was obtained by centrifugation after the solution aging for 24 h washed with deionized water and ethanol several times. Finally, the NaFeHCF particles were obtained after drying in a vacuum oven at 70°C overnight. To investigate the effect of synthesis condition on the structure and desalination performance of the material, the chelator concentration (0~0.5 mol/L), reaction temperature (25˚C, 60˚C, and 100˚C), and additional sodium salt (0~4 mol/L) were regulated during the synthesis process, and the specific parameters are given in the Table S1.

Desalination experiments

The working electrodes were prepared by casting a slurry containing the active material, Super P conductive agent, and polyvinylidene fluoride (PVDF) binder with a mass ratio of 7:2:1 on graphite paper, and then vacuum dried at 70°C overnight. The

solution conductivity during the desalination process was recorded using a conductivity meter (DDSJ-307F).

The desalination capabilities and reusability of electrodes during desalination process were evaluated by using a battery analyzer (Neware, China) in a three-electrode system, and the voltage range was -0.6~0.6 V (*vs* Ag/AgCl). The RCDB system was consisted of two NFHCF symmetrical electrodes and an anionic membrane (AME). Unless otherwise specified, the current density and electrolyte in the desalting experiments was 0.25 A/g and simulated seawater (1.0 M of NaCl solution), respectively. The specific capacity is calculated by the equation 1:

$$C = \frac{I \times t}{m} \tag{1}$$

$$\text{Capacity retention } (\%) = \frac{C_t}{C_0} \times 100 \tag{2}$$

where C is the specific capacity (mAh/g); m (g) is the mass of NaFeHCF composites; I and t are the current (mA) and time (h) in the charge-discharge process, respectively; C_0 and C_t are the initial specific capacity and the specific capacity after long-term runs, respectively.

The salt removal capacity (SRC, mg/g) and corresponding mean desalination rate (SRR, mg g^{-1} min^{-1}) are calculated by the following equations, respectively:

$$SRC = \frac{V \times (c_0 - c_t)}{m} \tag{3}$$

$$SRR = \frac{SRC}{t} \tag{4}$$

where V is the volume of the NaCl solution (L); c_0 and c_t are the initial concentration and desalinated concentration of ion, respectively; t is the desalination time (min).

The coulombic efficiency (CE) and charge efficiency (η) are calculated using the

following equations:

$$Coulomic\ efficiency\ (\%) = \frac{C_{i,d}}{C_{i,c}} \times 100 \quad (5)$$

where $C_{i,d}$ and $C_{i,c}$ are the specific capacity at the discharging and charging in the *i*th cycle, respectively; F is Faraday constant (96485 C/mol); M is the molar mass of NaCl (58.5 g/mol). To better reflect the desalting performance of NFHCF-x under different current densities, rate (mg g^{-1} min^{-1}) in Fig 3D are approximately calculated based on the assumption of 100% charge efficiency.

Characterization

Scanning electron microscopy (SEM, Quanta 650) was employed to elucidate the morphological features of the samples. Crystal structure of the as-prepared samples was recorded by an X-ray powder diffractometry (XRD, Haoyuan, DX-27 mini, China) with a Cu Kα radiation source from 10−90º. X-ray photoelectron spectroscopy (XPS) was accomplished via a Thermo Scientific K-Alpha spectrometer with an Al Kα source. Inductively coupled plasma optical emission spectrometer (ICP-OES, Avio 500, PerkinElmer) was used to test the ion in the treated solution. Thermogravimetry analysis (TGA) measurements were conducted on the TG/DTA8122 analyzer from 50 to 450°C at a rate of 10°C/min. The electrochemical experiments by cyclic voltammetry (CV) and electrochemical impedance spectroscopy (EIS) were conducted by using an electrochemical workstation (Corrtest, 129 CS350H, China) in a three-electrode system, composed of a counter electrode (carbon-fiber), a reference electrode (Ag/AgCl electrode) and electrolyte (1.0 M of

NaCl solution).

Table S1. Synthesis conditions for NFHCF samples.

Samples	Sodium citrate	Reaction temperature	Sodium chloride
NFHCF-0C	0 mol/L		
NFHCF-0.1C	0.1 mol/L		
NFHCF-0.2C	0.2 mol/L		
NFHCF-0.3C	0.3 mol/L	60˚C	1.0 mol/L
NFHCF-0.4C	0.4 mol/L		
NFHCF-0.5C	0.5 mol/L		
NFHCF-25˚C		25˚C	
NFHCF-60˚C	0.3 mol/L	60˚C	1.0 mol/L
NFHCF-100˚C		100˚C	
NFHCF-0			0.0 mol/L
NFHCF-1			1.0 mol/L
NFHCF-2	0.3 mol/L	60˚C	2.0 mol/L
NFHCF-3			3.0 mol/L
NFHCF-4			4.0 mol/L

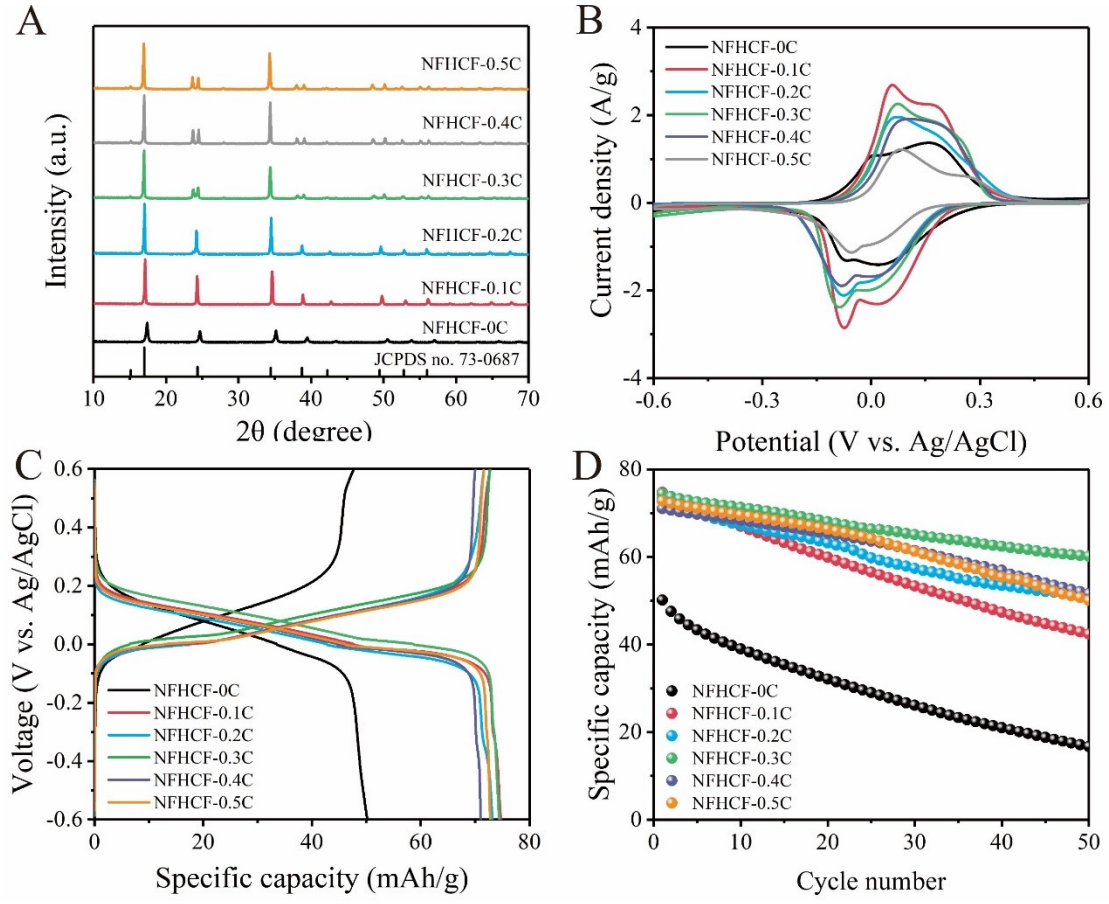

Fig S1. (A) XRD patterns, (B) CV curve at 1 mV/s, (C) charge-discharge curves, and (D) cycle performance of NaFeHCF prepared with different chelating doses.

Fig S1A exhibits the XRD patterns of the synthesized materials with different chelating agent doses (NFHCF-xC). The XRD pattern of NFHCF-0C can be indexed to the face-centered cubic structure of Prussian blue (JCPDS No: 73-0687). With higher doses of sodium citrate added in, the diffraction peaks show a trend of increasing intensity and left-shift. This is because the presence of chelating agent can slow down the crystallization rate and thereby improving the crystallinity of NaFeHCF; meanwhile, the increase of sodium content in the material causes the expanded cell size of crystal [1]. Moreover, with a further increase of dose (≥0.3 M), various diffraction peaks such as at 2θ= 24˚, 39˚, 50˚ and 56˚ split into a double peak

structure, which is attributed to the lattice distortion caused by the excessive sodium content in the material, thus converting the crystal structure from cubic phase to monoclinic phase.

The redox reaction process of NFHCF-xC was analyzed by CV measurements in Fig S1B. The redox peaks at -0.07/0.01 V and 0.03/0.16 V for NFHCF-0C are related to the oxidation/reduction of high-spin Fe^{3+}/Fe^{2+} couple coordinated with $(C\equiv N)^-$ by N atoms and low-spin Fe^{3+}/Fe^{2+} couple coordinated with $(C\equiv N)^-$ by C atoms, respectively [2]. Compared with the NFHCF-0C, the peak current density of the samples is obviously improved by the introduction of appropriate dose of sodium citrate, which indicates the higher capacity of Na^+ capture. Galvanostatic charge-discharge test was used to evaluate the sodium removal capabilities of different electrode samples at 0.25 A/g. As shown in Fig S1C, NFHCF-0C delivers an initial specific capacity of 50.2 mAh/g, while the initial specific capacity of the NFHCF-0.1C, NFHCF-0.2C, NFHCF-0.3C, NFHCF-0.4C, and NFHCF-0.5C improves to 74.7, 73.2, 74.5, 71.0 and 72.8 mAh/g, respectively. Fig S1D demonstrates that the capacity retention of NFHCF-0C is only 33.3% after 50 cycles; however, the capacity retention of the optimal NFHCF-0.3C is still more than 80%. This indicates that the appropriate dose of chelating agent can optimize the crystal structure of the material, thus significantly improving its desalination capacity and cycle performance.

On the other hand, the influence of reaction temperature was investigated. As shown in Fig S2A, with the increase in reaction temperature, there is no obvious change in the XRD pattern except for the slight decrease in peak intensity. CV curves

reveal that the peak current density of the material decreases obviously when the reaction temperature rose to 100˚C (Fig S2B). Similar to the CV analysis, NFHCF-25˚C delivers the initial specific capacity of 76.3 mAh/g, whereas the initial specific capacity of NFHCF-100˚C decreases to 69.8 mAh/g (Fig S2C). After 50 cycles, the capacity retention of NFHCF-25˚C, NFHCF-60˚C, and NFHCF-100˚C is 75.7%, 80.8%, and 66.2%, respectively (Fig S2D). Therefore, 60˚C is selected to be the optimal reaction temperature based on the balance of a relatively specific capacity and capacity retention.

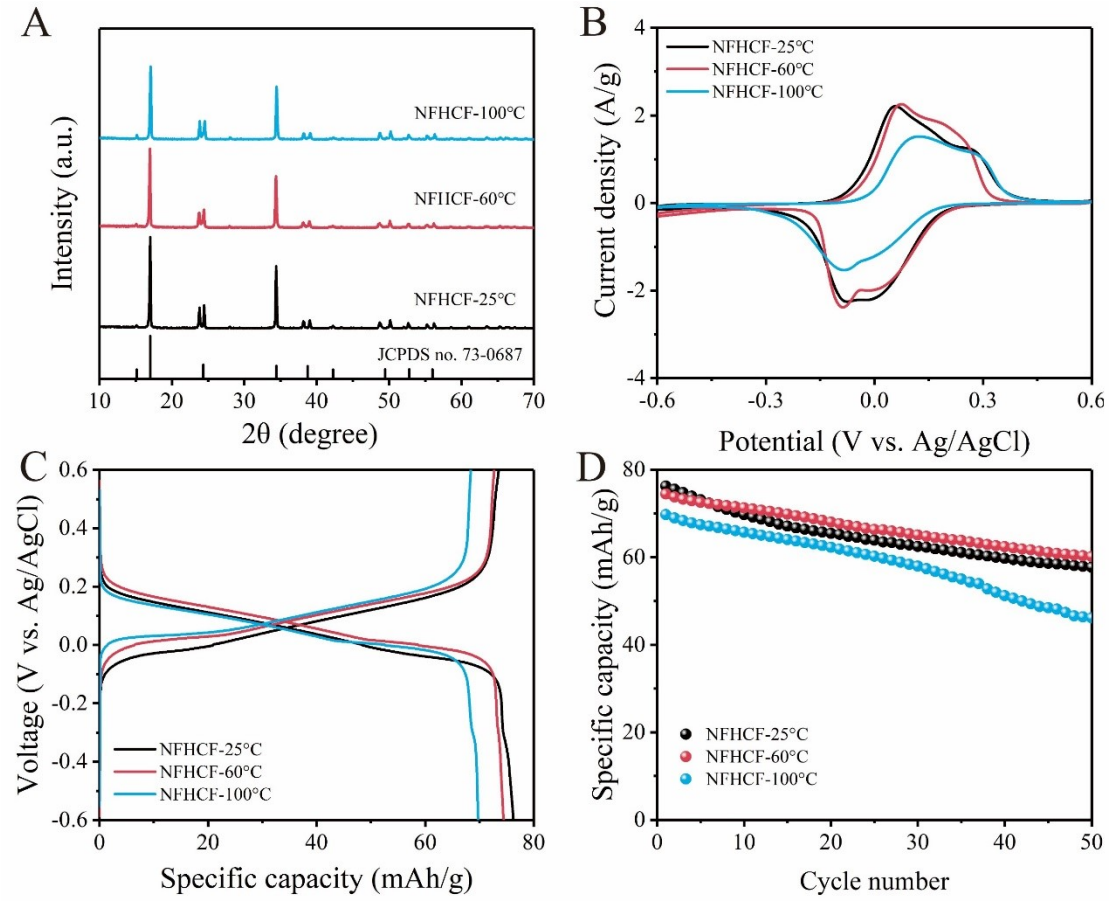

Fig S2. (A) XRD patterns, (B) CV curves at 1 mV/s, (C) charge-discharge curves, and (D) cycle performance of NaFeHCF prepared at different reaction temperature.

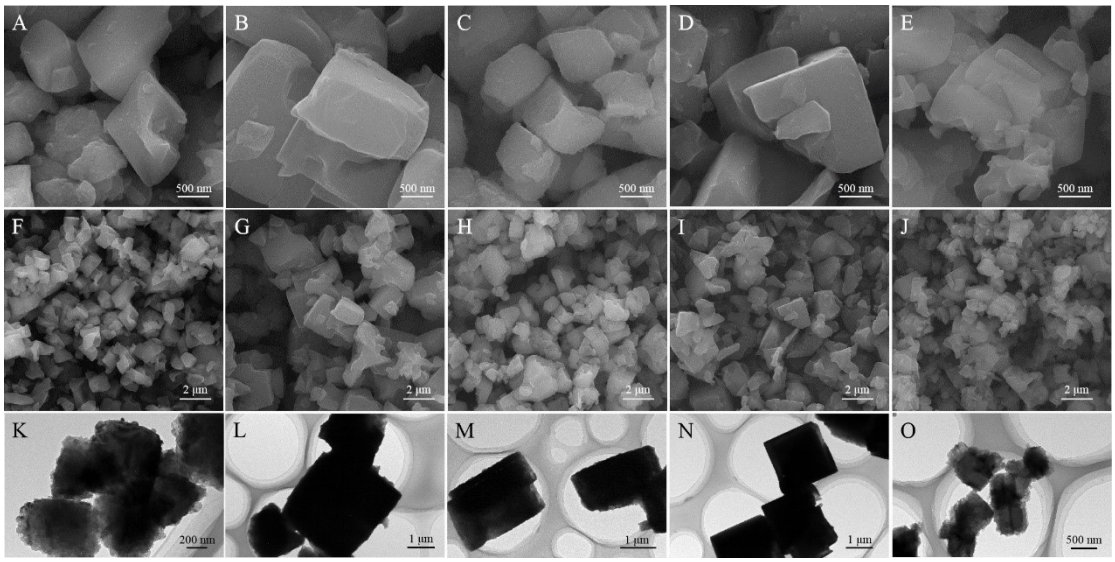

Fig S3. SEM images of (A), (F) NFHCF-0, (B), (G)NFHCF-1, (C), (H) NFHCF-2, (D), (I) NFHCF-3, and (E), (J) NFHCF-4; TEM images of (K) NFHCF-0, (L) NFHCF-1, (M) NFHCF-2, (N) NFHCF-3, and (O) NFHCF-4.

Table S2. The impedance parameters of the as-prepared NFHCF-x composites.

Samples	Rct (ohm)	σ (ohm/s$^{0.5}$)	D_{Na} (cm^2/s)
NFHCF-0	12.0	0.343	2.07×10^{-9}
NFHCF-1	1.01	0.150	2.86×10^{-9}
NFHCF-2	2.47	0.143	3.17×10^{-9}
NFHCF-3	2.66	0.217	1.37×10^{-9}
NFHCF-4	3.72	0.250	1.03×10^{-9}

Electrochemical impedance spectra (EIS) were performed on the pristine and cycled electrodes to evaluate the effects of experiment parameters on the electrical conductivity and ion diffusion of the electrodes. The linear relationship between Z' and $\omega^{-1/2}$ in the low-frequency range of the EIS spectra and its slope was determined as the Warburg factor (σ) related to the Na^+ diffusion coefficient (D_{Na}). The calculation formulas are as follows:

$$Z^{'} = R_{sl} + R_{ct} + \sigma\omega^{-1/2} \tag{6}$$

$$D_{Na} = \frac{R^2T^2}{2A^2n^4F^4C^2\sigma^2} \tag{7}$$

where R, T, and F are constants, A is the electrode area, n is the electron transfer number, C is the concentration of Na ions in the electrodes, and σ is the Warburg factor.

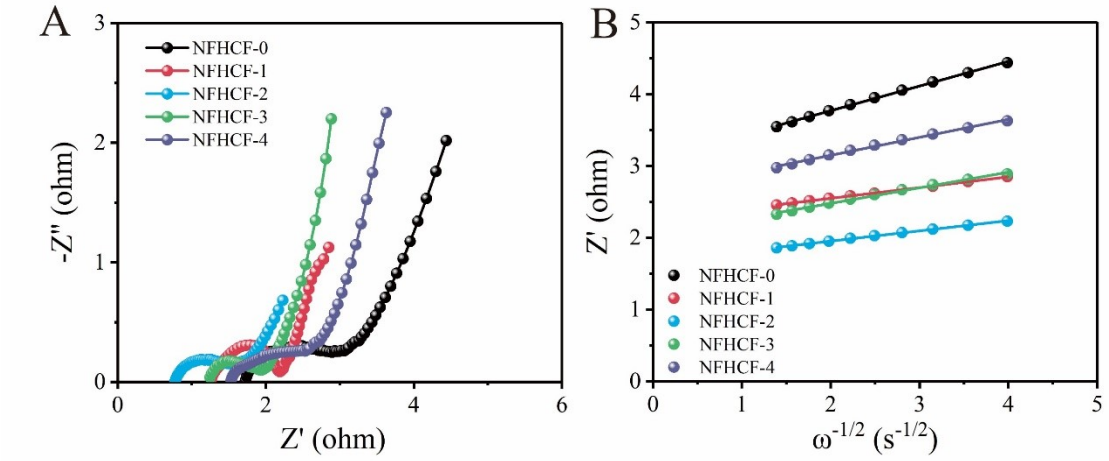

Fig S4. Nyquist plots of NFHCF-x electrode.

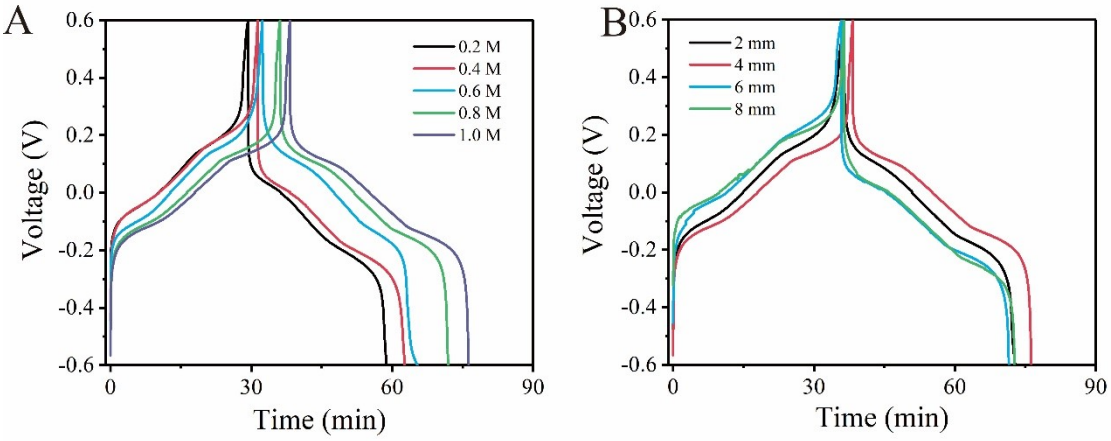

Fig S5. The voltage-time curves of NFHCF-2||NFHCF-2 RCDB after full activation at 0.1 A/g with (A) various initial NaCl concentrations and (B) various electrode spacing

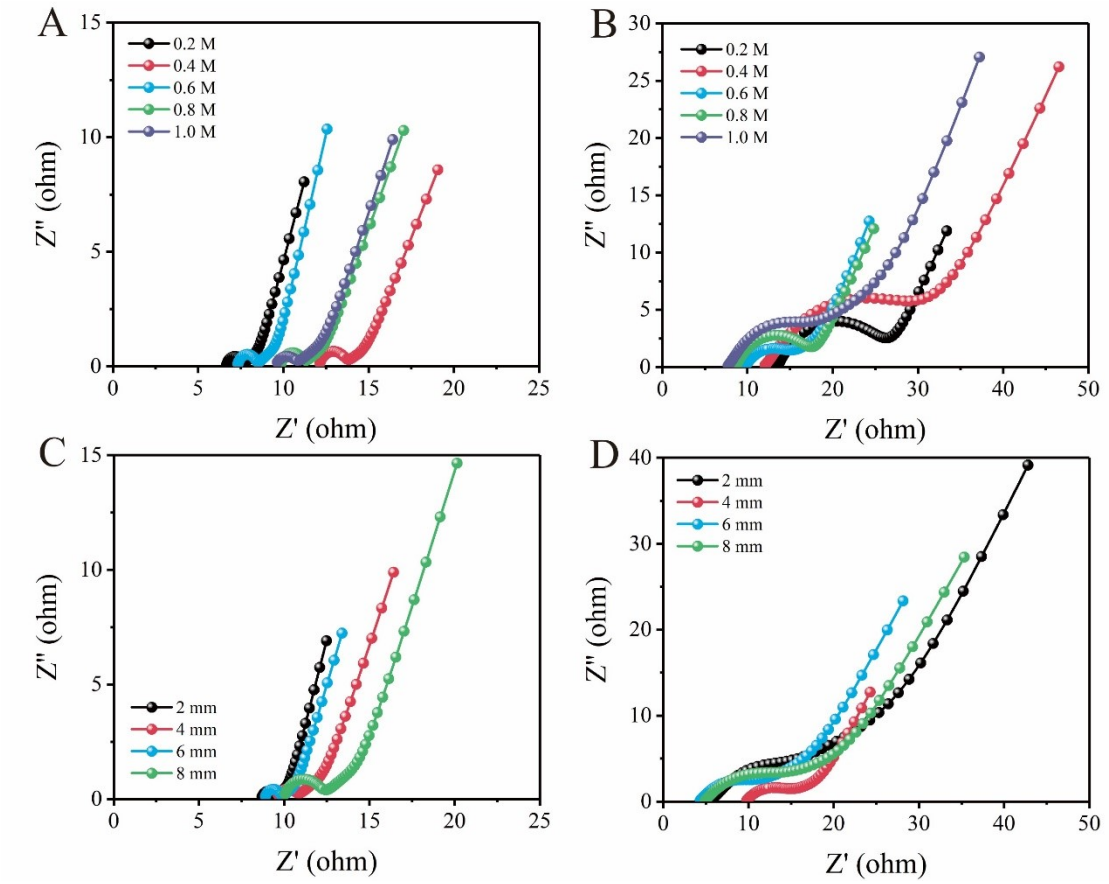

Fig S6. Nyquist plots of NFHCF-2 electrodes at various initial NaCl concentrations (A) before and (B) after cycle; Nyquist plots of NFHCF-2 electrodes at various electrode spacing (C) before and (D) after cycle

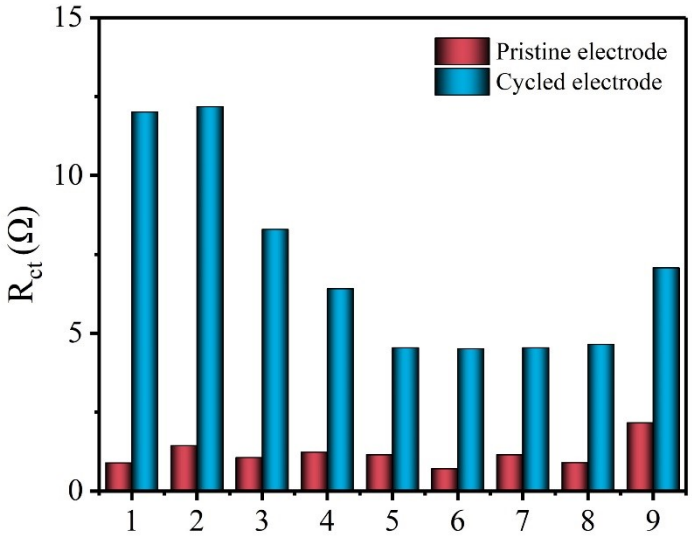

Fig S7. The impedance parameters before and after 150 cycles for devices with various NaCl concentrations (1: 0.2 M; 2: 0.4 M; 3: 0.6 M; 4: 0.8 M; 5: 1.0 M) and electrode spacing (6: 2 mm; 7: 4 mm; 8: 6 mm; 9: 8 mm)

EIS analysis was performed on the pristine electrode and the cycled electrode. As shown in Figs S6 and S7, the Rct of electrodes and the growth of Rct under the experimental conditions of 1.0 M NaCl and 4 mm electrode spacing, respectively, are lower. This indicates that NFHCF-2-based RCDB under these parameters can have higher desalination performance. Therefore, electrode spacing of 4 mm and NaCl concentration of 1.0 M were selected as the optimal operating parameters.

Table S3. Primary properties of natural seawater.

pH	Na^+ (mg/L)	Fe^{3+} (mg/L)	Mg^{2+} (mg/L)	Ca^{2+} (mg/L)
8.14	10101.62	/	622.66	74.91

Table S4. Comparison of the salt removal capacity (SRC), salt removal rate (SRR), energy consumption (EC) performance, charge efficiency and cycle stability on the reported electrochemical desalination system.

Electrode material	SRC (mg/g)	SRR (mg g^{-1} min^{-1})	EC (kWh/kg-NaCl)	Charge efficiency	Cycle number/ capacity retention	Ref.
Nafion-coated NaNiHCF||NaFeHCF	72	0.06	0.369	89.0%	100/94%	[3]
NaNiHCF||NaFeHCF	59.9	0.036	0.395	83%	100/91%	[4]
Flowerlike PB|| Flowerlike PB	101.3	~1.69	0.25	~71.1	60/93.3%	[5]
NaFeHCF@CNT ||NaFeHCF@CNT	82.97	1.38	0.360	83%	50/89.8%	[6]
NFHCF-2||NFHCF-2	108.9	2.22	0.056	78.4%	150/~100%	**This work**

References

1. Y. Liu, Y. Qiao, W. Zhang, Z. Li, X. Ji, L. Miao, L. Yuan, X. Hu and Y. Huang, *Nano Energy*, 2015, **12**, 386-393.
2. C. Xu, Z. Yang, X. Zhang, M. Xia, H. Yan, J. Li, H. Yu, L. Zhang and J. Shu, *Nano-Micro Letters*, 2021, **13**, 166.
3. J. Ahn, S. Kim, S.-i. Jeon, C. Lee, J. Lee and J. Yoon, *Desalination*, 2021, **500**, 114778.
4. J. Lee, S. Kim and J. Yoon, *ACS Omega*, 2017, **2**, 1653-1659.
5. A. Gong, Y. Zhao, X. Zhang, B. Liang, W. Zhang and K. Li, *Separation and Purification Technology*, 2022, **285**, 120333.
6. W. Zhang, X. Wei, X. Zhang, S. Huo, A. Gong, X. Mo and K. Li, *Separation*

and Purification Technology, 2022, **287**, 120483.